Orbital dynamics of high area-to-mass ratio spacecraft with J_2 and solar radiation pressure for novel Earth observation and communication services

Camilla Colombo[1], Charlotte Lücking[2], Colin R. McInnes[3]

Advanced Space Concepts Laboratory, University of Strathclyde, Glasgow, United Kingdom, G11XJ

This paper investigates the effect of planetary oblateness and solar radiation pressure on the orbits of high area-to-mass spacecraft. A planar Hamiltonian model shows the existence of equilibrium orbits with the orbit apogee pointing towards or away from the Sun. These solutions are numerically continued to non-zero inclinations and considering the obliquity of the ecliptic plane relative to the equator. Quasi-frozen orbits are identified in eccentricity, inclination and the angle between the Sun-line and the orbit perigee. The long-term evolution of these orbits is then verified through numerical integration. A set of 'heliotropic' orbits with apogee pointing in the direction of the Sun is proposed for enhancing imaging and telecommunication on the day side of the Earth. The effects of J_2 and solar radiation pressure are exploited to obtain a passive rotation of the apsides line following the Sun; moreover the effect of solar radiation pressure enables such orbits at higher eccentricities with respect to the J_2 only case.

Keywords: Frozen orbits, Heliotropic orbits, Solar radiation pressure, Earth's oblateness, Hamiltonian systems

I. INTRODUCTION

Current developments in system miniaturisation and network communication through wireless architectures will enable the use of swarms of 'smart dust' spacecraft, as distributed nodes of a sensor network for a range of future science missions [1, 2]. Such advances in miniaturisation developed for the terrestrial market allow the fabrication of operational spacecraft down to the dimensions of a single chip, with sensing, computing and communication capabilities [3, 4]. These are termed satellites-on-a-chip, 'smart dust' or SpaceChips [5]. Their small size reduces production costs and favours standardisation, as in the case of CubeSats, hence offering the benefit of the fabrication of vast numbers of devices for use in swarm applications. Moreover, miniaturisation overcomes limitations imposed by launch and deployment costs, since SpaceChips can be deployed in orbit from a conventional spacecraft. Increased launch opportunities and low manufacturing costs can reduce total mission cost and hence the employment of 'smart dust' devices can accept higher risk to investigate new phenomena or explore the harsh space environment. These advantages could form the basis for massive distributed space sensor networks, similar in scale to the early West Ford Needles project in 1963 [6]. The deployment of vast numbers of such 'SpaceChips' could enable future missions, such as global sensor networks for remote sensing, distributed communications, distributed space missions for multi-point, real-time sensing for space science [7] or deployment in the vicinity of a conventional spacecraft for diagnostic or even environmental purposes such as geo-engineering [8].

---

1 Corresponding author. Tel.: +44 (0)2380592319.
E-mail addresses: c.colombo@soton.ac.uk (C. Colombo), charlotte.lucking@strath.ac.uk (C. Lücking), colin.mcinnes@strath.ac.uk (C. McInnes).
2 Tel. +44 1415485937.
3 Tel. +44 1415482049.

However, such devices have a significantly higher area-to-mass ratio than conventional spacecraft due to their small length-scale [9]. For these spacecraft, surface perturbations, such as solar radiation pressure (SRP) and atmospheric drag are no longer negligible and rather than be counteracted, they can be exploited to generate new families of highly perturbed non-Keplerian orbits [10].

This paper investigates the passive orbital dynamics of high area-to-mass ratio spacecraft under the influence of SRP and the J_2 planetary oblateness. The effect of these perturbations on small dust particles has been studied extensively in the vast literature on the dynamics of dust in planetary systems [11-15]. These studies reveal interesting behaviours for dust in orbit at Mars or Saturn, and are focused on low eccentricity and low inclination orbits. Hamilton and Krivov [11] and Krivov and Getino [16] investigated the dynamics of coupling between solar radiation pressure and the planetary oblateness also at high eccentricities but low inclination orbits; although no planetary system shows such dust behaviour, the same method can be applied to the orbital dynamics of spacecraft with large area-to-mass ratios [16].

Contrary to many previous works, our investigation imposes no restriction on orbit eccentricity and inclination. Through a simplified planar model of the dynamics of the problem [11, 16], where the tilt of the Earth's equator relative to the ecliptic plane is neglected, it is possible to identify families of equilibrium orbits in-plane analytically. A Sun-synchronous condition is achieved passively such that the orbit apse-line is aligned with the Sun-line, without orbit control and the other in-plane orbital elements are constant or librate around an equilibrium value.

We then extend the analysis of these orbits by removing the assumption of a planar J_2 effect (i.e., zero planet obliquity). Starting from the conditions for the frozen orbits found analytically in the planar case, their long-term evolution is investigated with a 3D dynamical model, in terms of the secular variation of the orbital elements through the Gauss' equations. When the actual obliquity of the equator relative to the ecliptic is considered, long-term perturbations due to SRP appear in the out-of-plane Keplerian elements (i.e., inclination and anomaly of the ascending node). Therefore, the librational orbits identified analytically on the ecliptic plane will present out-of-plane oscillations, which can be exploited to displace a swarm of small spacecraft in a toroidal region around the Earth's equator.

In particular, the paper proposes a new set of quasi-frozen orbits at non-zero inclination for a swarm of small spacecraft for Earth observation and telecommunications applications. The effects of SRP and J_2 are exploited to maintain the spacecraft on a family of orbits with a Sun-pointing apogee, so that a large fraction of the orbit is spent on the day side for visible light imaging, or providing communications services during high demand daylight hours. This new set of inclined eccentric *heliotropic* orbits can be achieved with relatively small area-to-mass spacecraft, therefore passive Sun-pointing can be achieved by equipping a conventional spacecraft with near-term deployable reflective structures.

The analytical simplified planar model summarised in Section II is then substituted with a full three-dimensional model in Section III. Section IV identifies quasi-frozen orbits with non-zero eccentricity and inclination and analyses the connection with the planar case and the J_2 only case. Finally, a set of heliotropic elliptical orbits is proposed in Section V for enhancing Earth observation and telecommunication services.

II. PLANAR MODEL OF THE ORBITAL DYNAMICS

II.I. Simplified planar dynamics

The two-body dynamics of a spacecraft with high area-to-mass ratio perturbed by the gravitational potential due to oblateness J_2 and by the effect of solar radiation pressure forms a Hamiltonian system. The secular rate of change of the orbital elements due to SRP and J_2 is given for example by Hamilton and Krivov [11] and Krivov and Getino [16] as

$$\frac{de}{d\lambda_{Sun}} = -C\sin\phi\sqrt{1-e^2}$$

$$\frac{d\phi}{d\lambda_{Sun}} = -C\cos\phi\frac{\sqrt{1-e^2}}{e} + \frac{W}{\left(1-e^2\right)^2} - 1 \tag{1}$$

where e is the eccentricity, and ϕ represents the angle between the Sun-Earth line and the direction of the orbit pericentre ($\phi = \tilde{\omega} - \left(\lambda_{Sun} - \pi\right)$ where $\tilde{\omega}$ defines the longitude of the pericentre and λ_{Sun} the true longitude of the Sun), as shown in Fig. 1.
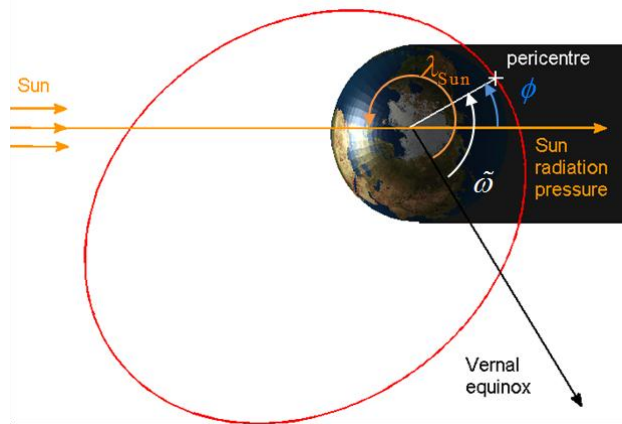
Fig. 1:   Planar orbit geometry.

Note that Eq. (1) considers a planar problem only, i.e. the orbit has zero inclination and the equatorial plane is assumed to be in the ecliptic (i.e., the obliquity angle of the ecliptic with respect to the equator is set to zero). Moreover, the effect of eclipses is neglected. As a consequence, the secular variation of semi-major axis and inclination is zero. These equations are governed by the solar radiation pressure parameter C and the oblateness parameter W, both of which dependent on the semi-major axis a

$$C = \frac{3}{2}a_{SRP}\frac{a^2}{\mu_{Earth}}\frac{n}{n_{Sun}}$$

$$W = \frac{3}{2}J_2\frac{R_{Earth}^2}{a^2}\frac{n}{n_{Sun}} \tag{2}$$

where a_{SRP} is the characteristic acceleration due to SRP $a_{SRP} = p_{SR}c_R A_{Sun}/m$ with $p_{SR} = 4.56\times10^{-6}\,\text{N/m}^2$ the solar pressure at 1 AU, c_R the reflectivity coefficient, taken equal to 1.8 in this paper, A_{Sun} is the area exposed to the Sun, and

m is the mass of the body. In the expression for the oblateness parameter W, $J_2 = 1.083 \cdot 10^{-3}$ denotes the second zonal harmonic coefficient and R_{Earth} is the mean radius of the Earth. n_{Sun} is the orbital angular velocity of the Earth around the Sun (circular Earth orbit is adopted) and $n = \sqrt{\mu_{Earth}/a^3}$ is the orbit angular velocity of the body on its orbit, where μ_{Earth} the gravitational constant of the Earth.

II.II. *Heliotropic* and *antiheliotropic* orbits

Eq. (1) allows as an integral of motion, the Hamiltonian, which is fixed by the initial condition of the orbit:

$$H = -\sqrt{1-e^2} + Ce\cos\phi - \frac{W}{3\left(1-e^2\right)^{3/2}} \tag{3}$$

Eq. (3) describes the particle's trajectory in the e-ϕ phase space as analysed by Hamilton and Krivov [11] and Krivov and Getino [16]. The Hamiltonian in Eq. (3) allows a maximum of three stationary points (i.e., $de/d\lambda_{Sun} = 0$ and $d\phi/d\lambda_{Sun} = 0$), one stable equilibrium at $\phi = 0$, one stable equilibrium at $\phi = \pi$ and one hyperbolic equilibrium (or saddle point) at $\phi = \pi$. The existence of these three stationary points and their eccentricity depends on the orbit semi-major axis and the area-to-mass of the spacecraft, which determine the SRP and J_2 parameters C and W in Eqs. (2).

Fig. 2 shows the evolution of the eccentricity of the $\phi = 0$ and $\phi = \pi$ stationary points as function of the semi-major axis for different area-to-mass ratios. At low semi-major axis, only the equilibrium at $\phi = 0$ exists (see light blue dot in Fig. 2a), this is mainly due to the interaction of the SRP perturbed dynamics, with the effect of non-sphericity of the Earth. This explains the limited eccentricity of this equilibrium point. The evolution of initial conditions chosen in the neighbourhood of this point will exhibit a librational or rotational evolution in the phase space around the stable equilibrium. The separatrix between librational or rotational evolution is represented by the line passing through $e = 0$ (bold line in Fig. 2a). For increasing semi-major axis the stable equilibrium at $\phi = \pi$ and the saddle point at $\phi = \pi$ appear as visible in Fig. 2b (light blue dots). In this case, both the line passing through $e = 0$ and the line passing through the saddle point are separatrices of the different possible behaviours (bold lines in Fig. 2b).

Higher area-to-mass ratios move the stationary points to higher values of the eccentricity at a fixed semi-major axis (see second and third rows of Fig. 2) and lead to a drift of the transition from one behaviour to another at higher semi-major axis (compare for example Fig. 2b with Fig. 2h). Finally, note that not all values of eccentricity are feasible for a given semi-major axis a, since the orbit perigee cannot move below one Earth radius, hence the eccentricity cannot exceed its critical value:

$$e_{crit} = 1 - \frac{R_{Earth}}{a}$$

Fig. 3 summarises all possible equilibria in the phase space for different values of area-to-mass ratio. The continuous lines at small semi-major axis represent the stationary solution at $\phi = 0$. In correspondence to this equilibrium point and for all librational conditions around it, the orbit apocentre is always pointing in the direction of the Sun, as inferred from Fig. 1. We will refer to this condition as *heliotropic orbits*, a term used by Hedman et *al.* and Burt et *al.* for the Cassini "charming" ringlet [14, 15]. The dashed and dotted lines in Fig. 3 indicate respectively the equilibrium at $\phi = \pi$ and the

saddle at $\phi = \pi$, which converge to the same eccentricity in correspondence to a specific semi-major axis (coloured circle). The equilibrium point at $\phi = \pi$ and all the librational behaviours around it correspond to orbits with the apocentre always pointing away from the Sun, or *antiheliotropic orbits*. The blue line in correspondence to a zero area-to-mass represents the case in which J_2 is the only perturbation (i.e., $C = 0$). If the effect of SRP is negligible (i.e., conventional spacecraft), the condition of Sun-following can be written analytically as for example ref. [11] and, unlike the J_2+SRP case, can be achieved at any orientation of the orbit apse-line with respect to the Sun:

$$e_{\phi\text{-syn } J_2} = \sqrt{1 - \sqrt{W}} \tag{4}$$

where the dependence on the semi-major axis is in the parameter W. The solution in Eq. (4) has been proposed by Draim et *al.* for forcing the apogee of the ellipse in the equatorial plane to remain oriented with respect to the Earth-Sun line throughout the year [17]. The advantage of this kind of heliotropic orbit is in the fact that a larger fraction of the orbit is spent on the day side of the Earth, since the spacecraft is travelling at lower speed near apogee with applications for Earth observation and communications.

It is noteworthy that the use of a spacecraft with non-negligible area-to-mass would allow heliotropic orbits of a given semi-major axis to have a greater eccentricity, therefore enabling a larger fraction of the orbit during daylight hours. The orbit eccentricity can be increased up to the maximum limit of the critical eccentricity represented by the shaded area in Fig. 3. Finally note that Eq. (4) represents the boundary between the equilibrium at $\phi = 0$ and the two stationary points at $\phi = \pi$ in the case of J_2+SRP.

a) $a = 11,000$ km, $A/m = 5$ m^2/kg   b) $a = 14,864$ km, $A/m = 5$ m^2/kg   c) $a = 18,000$ km, $A/m = 5$ m^2/kg

d) $a = 11,000$ km, $A/m = 10$ m^2/kg   e) $a = 14,864$ km, $A/m = 10$ m^2/kg   f) $a = 18,000$ km, $A/m = 10$ m^2/kg

g) $a = 11,000$ km, $A/m = 20$ m^2/kg   h) $a = 14,864$ km, $A/m = 20$ m^2/kg   i) $a = 18,000$ km, $A/m = 20$ m^2/kg
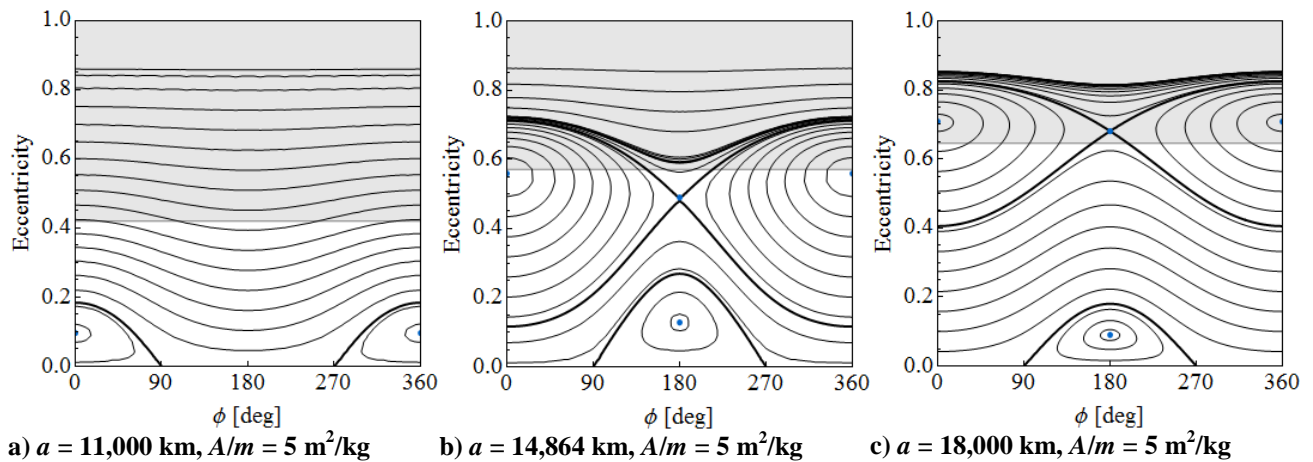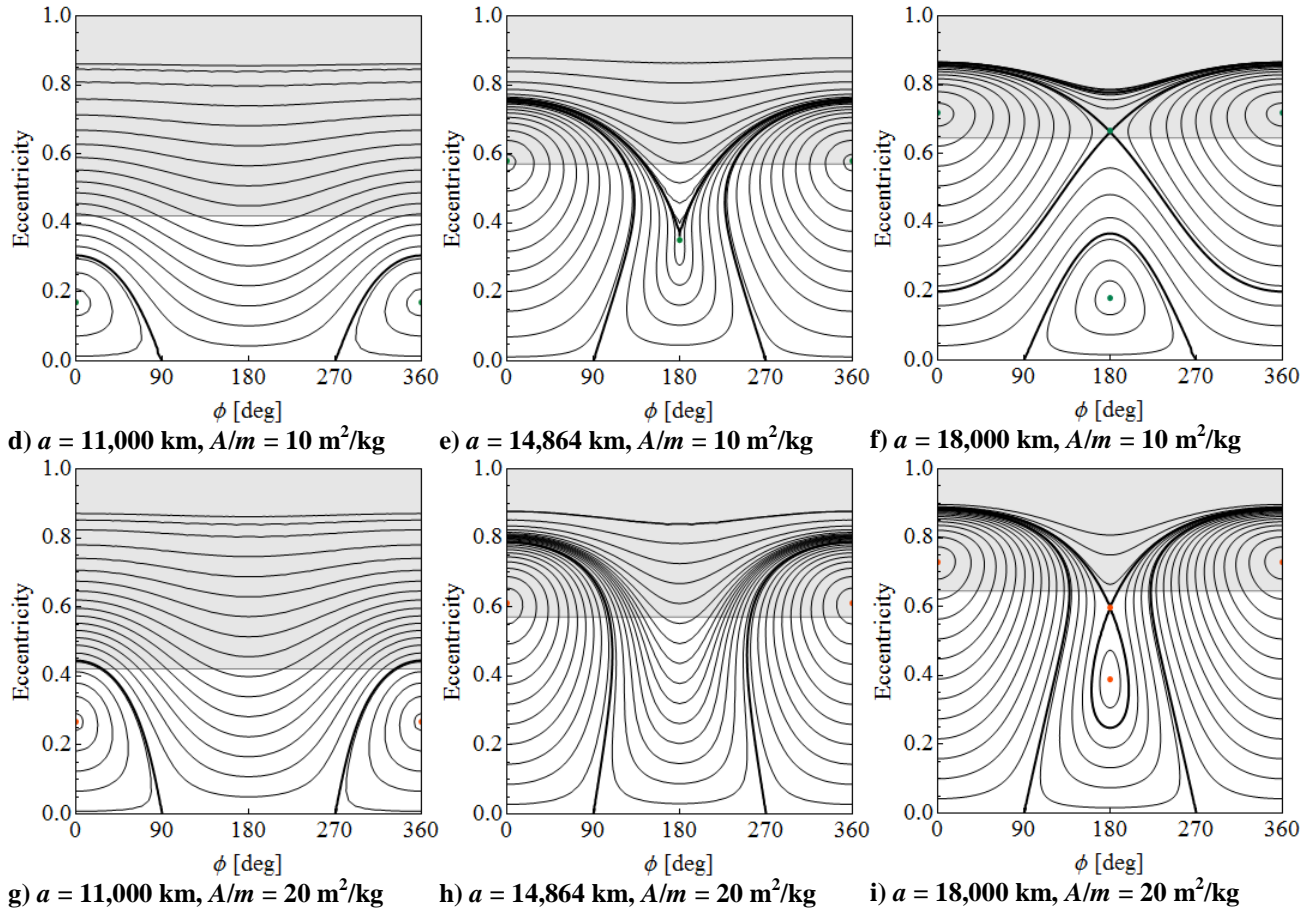
Fig. 2: **Eccentricity-ϕ phase space evolution for the planar simplified case of J_2+SRP. The bold lines represent the separatrices in correspondence of the saddle point and zero eccentricity Hamiltonian, the shaded area marks orbit heights lower than one Earth radius. Semi-major axis of 11,000 km (first column), 14,864 km (second column) and 18,000 km (third column). Area-to-mass of 5 m^2/kg (first row), 10 m^2/kg (second row) and 20 m^2/kg (third row).**
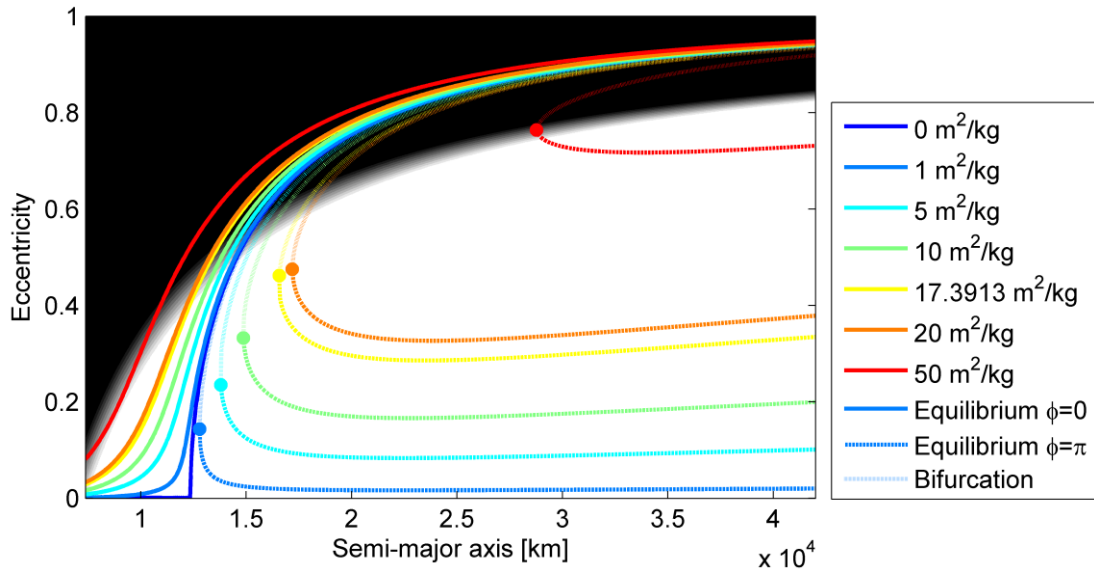
Fig. 3: Eccentricity of the stationary points at $\phi=0$ (bold continuous line) and $\phi=\pi$ (dotted and bold dashed lines) as function of the semi-major axis for different area-to-mass ratios and reflectivity coefficient of 1.8. The blue line represents the J_2 case only.

III. THREE DIMENSIONAL MODEL OF THE ORBITAL DYNAMICS

In the following section the simplified assumption of a zero obliquity angle ε of the ecliptic with respect to the equator will be removed. Therefore, the five Keplerian elements a, e, i, Ω and ω measured in an inertial equatorial system are necessary to describe the shape and orientation of the orbit as depicted in Fig. 4 (we are not interested in the true anomaly as we do not consider here the position of the spacecraft on its orbit). In the three-dimensional case the longitude of the Sun measured on the ecliptic plane from the vernal equinox λ_{Sun} is needed and the initial position of the Sun becomes another variable of the problem.
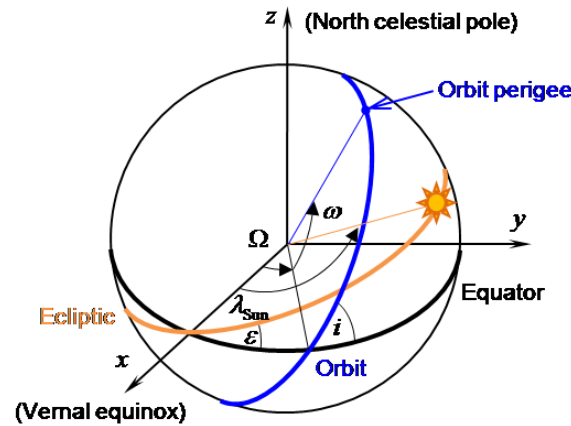
Fig. 4: 3D orbit geometry.

The three dimensional dynamics under the effect of J_2 and SRP was derived by Krivov [16] in a set of non-singular Lagrangian elements defined as

$$
\begin{aligned}
h &= e\cos(\omega+\Omega) \\
k &= e\sin(\omega+\Omega) \\
p &= \sin i \cos\Omega \\
q &= \sin i \sin\Omega
\end{aligned}
\tag{5}
$$

We report Krivov's equation in the following so that we have the chance to correct a typo in Krivov's paper (in the SRP term of $dk/d\lambda_{Sun}$):

$$\frac{dh}{d\lambda_{Sun}} = -kW \frac{5I^2 - 2I - 1}{2E^4} +$$

$$-\frac{C}{E(1+I)}\left((p - Hh)q\cos\lambda_{Sun} + \left(E^2(1+I) - p(p-Hh)\right)\cos\varepsilon\sin\lambda_{Sun} + \left(E^2(1+I)p - IKk\right)\sin\varepsilon\sin\lambda_{Sun}\right)$$

$$\frac{dk}{d\lambda_{Sun}} = +hW \frac{5I^2 - 2I - 1}{2E^4} +$$

$$+\frac{C}{E(1+I)}\left((q - Hk)p\cos\varepsilon\sin\lambda_{Sun} + \left(E^2(1+I) - q(q-Hk)\right)\cos\lambda_{Sun} - \left(E^2(1+I)q + IKh\right)\sin\varepsilon\sin\lambda_{Sun}\right)$$

$$\frac{dp}{d\lambda_{Sun}} = +qW \frac{1}{E^4} + \frac{C}{E(1+I)}\left(Hp - (1+I)k\right)\left((p\cos\varepsilon - I\sin\varepsilon)\sin\lambda_{Sun} - q\cos\lambda_{Sun}\right)$$

$$\frac{dq}{d\lambda_{Sun}} = -pW \frac{1}{E^4} + \frac{C}{E(1+I)}\left(Hq - (1+I)k\right)\left((p\cos\varepsilon - I\sin\varepsilon)\sin\lambda_{Sun} - q\cos\lambda_{Sun}\right)$$

(6)

where

$$E = \sqrt{1 - h^2 - k^2}$$
$$I = \sqrt{1 - p^2 - q^2}$$
$$H = hp + kq$$
$$K = hq - kp$$

We note that the semi-major axis remains constant if we neglect eclipses.

III.I. Three-dimensional phase space

When we consider the actual value of the ecliptic obliquity, in the case of the Earth $\varepsilon = 23.4393$ deg, this results in more complex coupled dynamics, because the solar radiation pressure causes a non-zero variation of all the four Lagrangian elements in Eq. (6) if acting on an orbit out of the ecliptic plane, whereas the effect of the J_2 term presents a simplified form exclusively for orbits on the Earth's equator, for which Ω and ω can be simply summed up. However, if we adopt a three-dimensional definition of the angle ϕ as

$$\phi = \Omega + \omega - (\lambda_{Sun} - \pi)$$

the phase space dynamics observed in the simplified planar case can still be recognised for increasing but limited values of the angle ε (ε less than 30° [18]). This can be appreciated in Fig. 5 which shows the evolution in the eccentricity-ϕ phase space for non-zero values of the ecliptic obliquity. Note that, the angles Ω, ω and λ_{Sun} do not lie on the same plane (i.e., i and ε are not zero), however the definition of the angle ϕ is quite close to the correct three-dimensional trigonometric angle if i and ε are not too high.
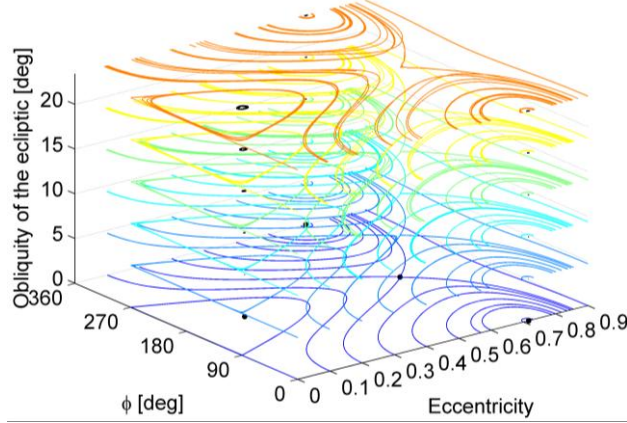
Fig. 5:   Sensitivity on the ecliptic obliquity ε (a= 18,000 km and A/m = 10 m^2/kg).

IV. QUASI-FROZEN ORBITS IN THE 3D DYNAMICS

Fig. 5 suggests that frozen or quasi-frozen solutions may exist as well in the three-dimensional J_2 and SRP case. Despite that an exact solution (i.e., frozen orbit) does not exist if the SRP parameter C is non-zero, the hypothesis of quasi-frozen orbits was verified numerically by minimising the cost function

$$\min_{\{e,\, i,\, \Omega,\, \omega\}} \left[w_e \left| de/d\lambda_{\text{Sun}} \right| + w_\phi \left| d\phi/d\lambda_{\text{Sun}} \right| + w_i \left| di/d\lambda_{\text{Sun}} \right| \right] \tag{7}$$

where the variation of eccentricity, ϕ and inclination can be obtained from Eqs. (5) and (6) as

$$\frac{de}{d\lambda_{\text{Sun}}} = \frac{h\dfrac{dh}{d\lambda_{\text{Sun}}} + k\dfrac{dk}{d\lambda_{\text{Sun}}}}{\sqrt{h^2+k^2}}$$

$$\frac{d\phi}{d\lambda_{\text{Sun}}} = \frac{h\dfrac{dk}{d\lambda_{\text{Sun}}} + k\dfrac{dh}{d\lambda_{\text{Sun}}} - \left(h^2+k^2\right)}{h^2+k^2} \tag{8}$$

$$\frac{di}{d\lambda_{\text{Sun}}} = \frac{p\dfrac{dp}{d\lambda_{\text{Sun}}} + q\dfrac{dq}{d\lambda_{\text{Sun}}}}{\sqrt{1-p^2-q^2}\sqrt{p^2+q^2}}$$

and w_e, w_ϕ, w_i are weight parameters introduced to treat this multi-objective minimisation problem (the three equations of system Eq. (8) must be zero) as a single-objective minimisation. A global multi-start approach is adopted. A local algorithm is started from several points randomly distributed over the entire domain of eccentricity, arguments of perigee-Sun displacement and inclination. Starting from each point on the mesh, a local minimisation is performed numerically, through a subspace trust-region method, based on the interior-reflective Newton method [19, 20]. Another variable of the problem would be the orbit semi-major axis; in fact, as seen in Fig. 2 this determines the eccentricity value of the stationary points. However, to keep the problem simple, we examine here the solution at a specific semi-major axis, leaving the extension to an extended range of orbit energies to a future work.

IV.I. Sun-following orbits under the effect of J_2 only

Before looking at the solutions of the minimisation in Eq. (7) when both SRP and J_2 influence the spacecraft motion, it is possible to find an analytical solution for Sun-following orbits with non-zero inclination for conventional spacecraft (i.e., effect of SRP negligible, hence $C = 0$) in the Earth vicinity (J_2 effect non negligible)

$$\frac{d\Omega}{d\lambda_{Sun}} + \frac{d\omega}{d\lambda_{Sun}} - 1 = 0$$

where the solution is given by:

$$i_{\phi\text{-syn}\,J_2} = \arccos\left[\frac{1}{5} \pm \frac{\sqrt{2}\sqrt{(5W)(1 - 2e^2 + e^4) + 3W^2}}{5W}\right] \tag{9}$$

where the plus sign identifies the prograde orbit (i.e., $i < 90\deg$) and the minus sign identifies the retrograde orbit (i.e., $i > 90\deg$). Note that the dependency on the semi-major axis is within the parameter W.

The solution of Eq. (9) is represented in Fig. 6 for different semi-major axes. Note that condition Eq. (9) is different than the condition of Sun-synchronicity which requires instead that only the change in anomaly of the ascending node equals the rate of rotation of the Earth around the Sun $d\Omega/d\lambda_{Sun} - 1 = 0$. The condition of Sun-synchronicity ensures the same lighting conditions on the orbit [21], while the Sun-following condition Eq. (9) guarantees that the line of apsides is at a constant orientation with respect to the Sun. More precisely, the initial right ascension of the orbit apogee or perigee point measured on the ecliptic plane with respect to the Sun is maintained. If the orbit has a non-zero inclination, the orbit apogee or perigee will rotate on the orbit plane (that is at constant inclination in an Earth equatorial system), but will be always on the dayside or nightside of the Earth with respect to the Sun. This orbit represents the extension of Eq. (4) for non-zero inclination and can be exploited for observation or telecommunications if the initial orientation is chosen as heliotropic (i.e., Sun-pointing apogee).
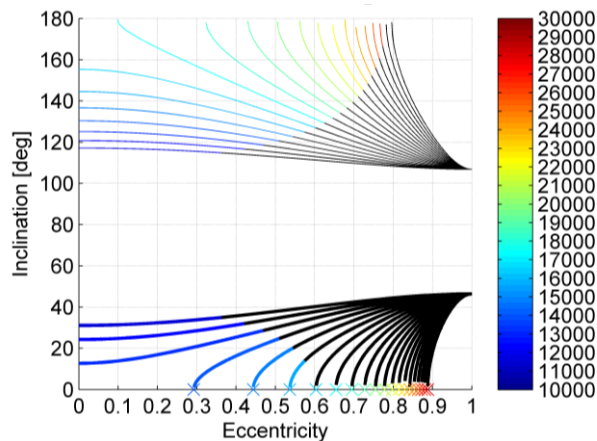
Fig. 6: **Sun-following orbits in the Earth's vicinity (J_2 only). The shaded part of the line indicates eccentricity greater than the critical value. The cross symbol is the planar solution Eq. (4).**

IV.II. Three dimensional frozen orbits with SRP and J_2

Also in the three-dimensional case, the J_2 only solution can be extended to higher eccentricities through the exploitation of SRP. However, as already pointed out at the beginning of Section IV, an exact solution does not exist but only quasi-frozen orbits can be found numerically. We fix a specific value of semi-major axis $a = 18,000$ km and area-to-mass $A/m = 17.39$ m^2$/kg$ [4]. The stationary points in the simplified planar model are reported in Fig. 7. We are aware that for this choice of a and A/m the equilibrium point at $\phi = 0$ is not feasible (i.e., $e > e_{\text{crit}}$). However, we are interested, at this point, only in studying the extension of these equilibria for non-zero inclinations. In Section V the actual orbit design will be selected.

Fig. 8 represents the extension of the stationary points in Fig. 7 for non-zero eccentricity at a fixed value of semi-major axis. The numerical solution of the minimisation problem in Eq. (7) identifies respectively quasi-frozen orbits at $\phi = \pi$ (blue crosses), quasi-frozen orbits at $\phi = 0$ (green dots) and saddle points at $\phi = \pi$ (red stars). Note that the extension of the stationary points at non-zero inclination is not a well-defined line because an exact solution does not exist.
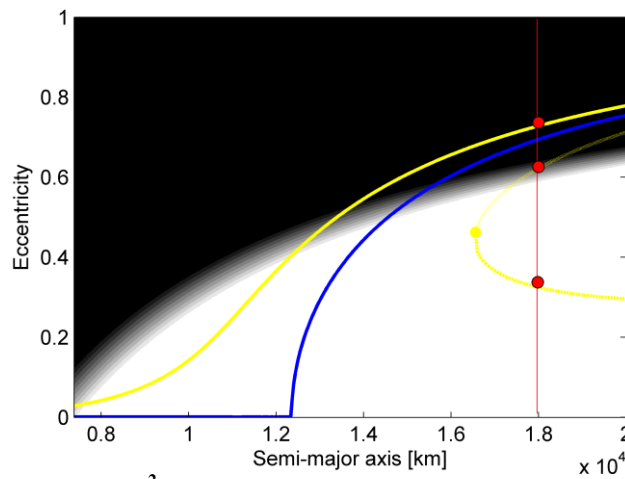
Fig. 7: Stationary points for A/m=17 m^2/kg and reflectivity coefficient of 1.8. The positions of the stationary points in correspondence of a = 18,000 km are highlighted with the red line. Starting from the lower eccentricity the three red points represent the equilibrium at ϕ=π, the saddle at ϕ=π and the equilibrium at ϕ=0.
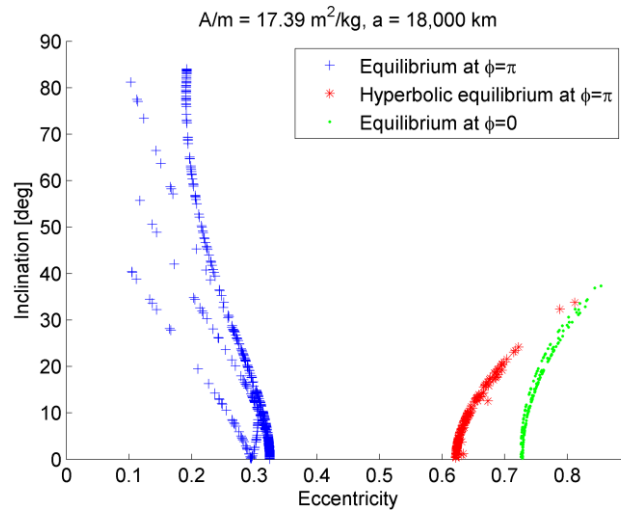
Fig. 8: **Quasi-frozen orbits at non-zero inclination under SRP and J_2 for A/m = 17.39 m^2/kg and a = 18,000 km: sun-pointing perigee orbits (blue), sun-pointing apogee orbits (green) and saddle (red).**

Each point in Fig. 8 identifies an initial condition for which the sum of the variation of eccentricity, inclination and solar radiation-perigee angle is at its minimum. These solutions are quasi-frozen orbits. The solutions identified through Eq. (7) are now used as initial condition for a numerical propagation of Eqs. (6), forward in time, over a period of 20 years. The numerical integration of Eqs. (6) is performed through an adaptive step-size Runge-Kutta-Fehlberg integration scheme integrator with a six stage pair of approximation of the fourth and fifth order [22], with absolute and relative tolerance of 3×10^{-14}.

IV.III. <u>Sun-pointing perigee quasi-frozen orbits</u>

The numerical integration of the initial conditions represented by the blue crosses in Fig. 8 shows an oscillation of the orbital elements that remains limited throughout the entire integration period. Specifically, for low values of inclination, the phase space evolution maintains a clear planar structure visible in the eccentricity-ϕ phase, as shown in an example in Fig. 9a (the initial condition for this integration is: $i_0 = 2.03 \deg$, $e_0 = 0.299$). All the orbits maintain their Sun-pointing perigee condition throughout the integration, showing oscillations around the equilibrium condition $\phi = \pi$ of less than one year period [23]. The vertical structure is characterised by oscillation of the inclination of a period between 3 and 4 years with a limited magnitude around the initial quasi-frozen condition (see for example Fig. 9b).
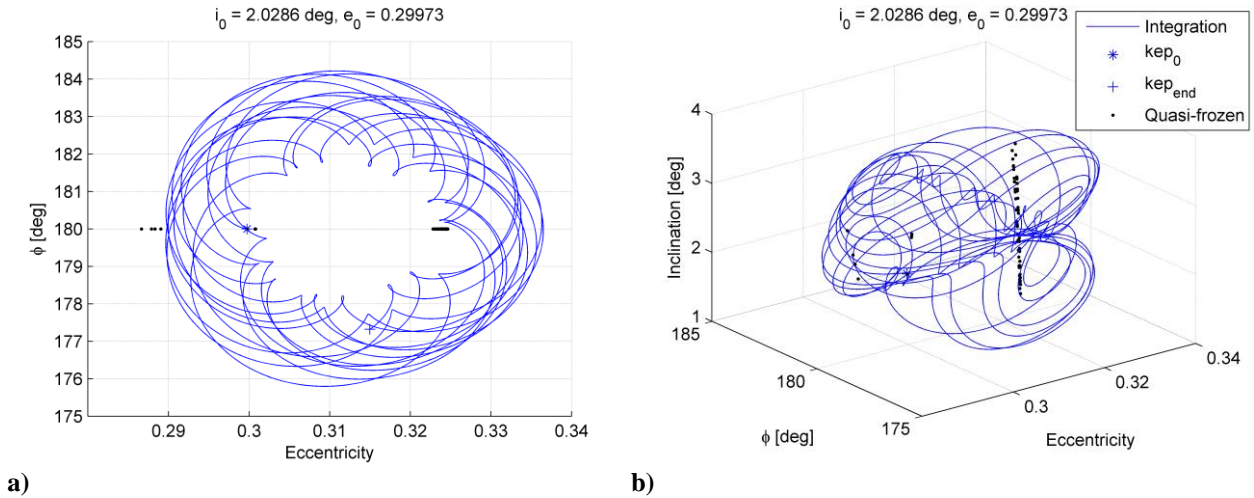
Fig. 9: Evolution of one condition of antiheliotropic orbit: a) planar structure, b) 3D structure.

For higher values of the initial inclination, the coupling between the planar and vertical structure becomes more visible and the oscillation around the initial quasi-frozen condition presents a greater amplitude. This is visible from Fig. 10 which represents the maximum (cross symbol) and minimum (diamond symbol) of the inclination (Fig. 10a) and eccentricity (Fig. 10b) around the initial condition (dot symbol). At high initial inclinations close to 90 degrees the interaction between the planar and vertical structure becomes predominant, causing large oscillations in the eccentricity which reaches the separatrix line which passes for $e = 0$. However, all initial conditions continue librating or rotating around the quasi-frozen solution identified.
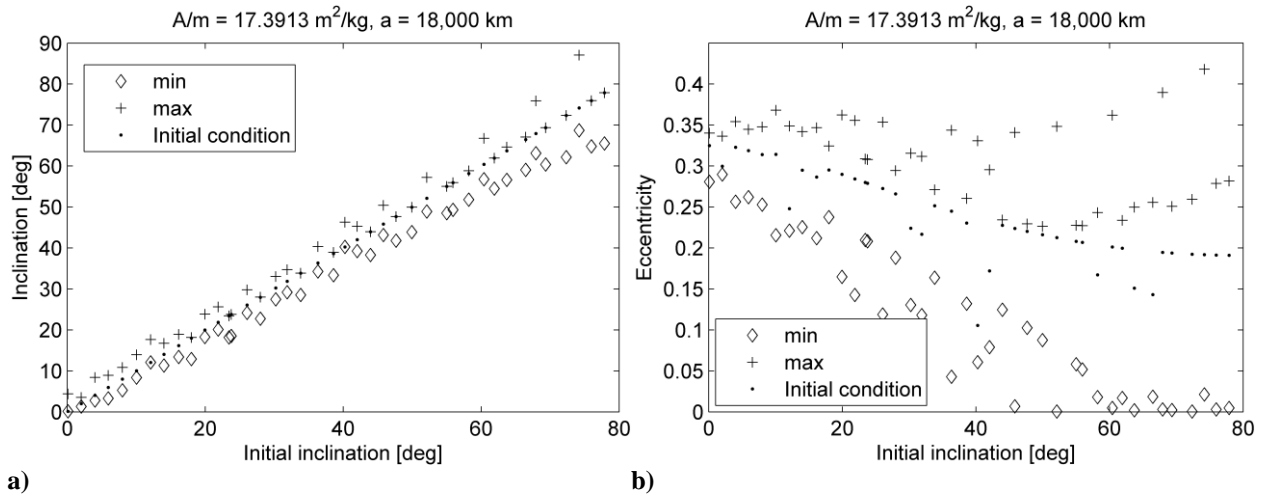
Fig. 10: Oscillation of (a) inclination and (b) eccentricity for Sun-pointing perigee orbits (Minimum: diamond; Maximum: cross). The quasi-frozen conditions (dots) are used as initial conditions for a 20 years numerical integration.

IV.IV. Sun-pointing apogee quasi-frozen orbits

Fig. 11 summarises the results of the long-term integration of the initial conditions identifying three-dimensional Sun-pointing apogee orbits or heliotropic orbits (green dots in Fig. 8). For values of initial inclination below 15 degrees, the 20 year numerical integration maintains limited eccentricity and inclination around the quasi-frozen condition (an example is given in Fig. 12 for $i_0 = 17.95 \, \mathrm{deg}$, $e_0 = 0.75$). Some initial conditions at higher values of the initial inclination reach the separatrix line, hence the transition from librational around the equilibrium at $\phi = 0$ to rotational. This explains the higher amplitude of the inclination and eccentricity oscillations for some initial conditions in Fig. 11. This result suggests that, as expected, the phase space structure in the planar simplified case becomes more and more distorted as the inclination increases; hence it can transit from one behaviour (i.e., librational) to the adjacent one (i.e., rotational) during long-term orbit evolution. At higher inclinations the initial position of the Sun plays an important role in the following evolution.

a)   b)
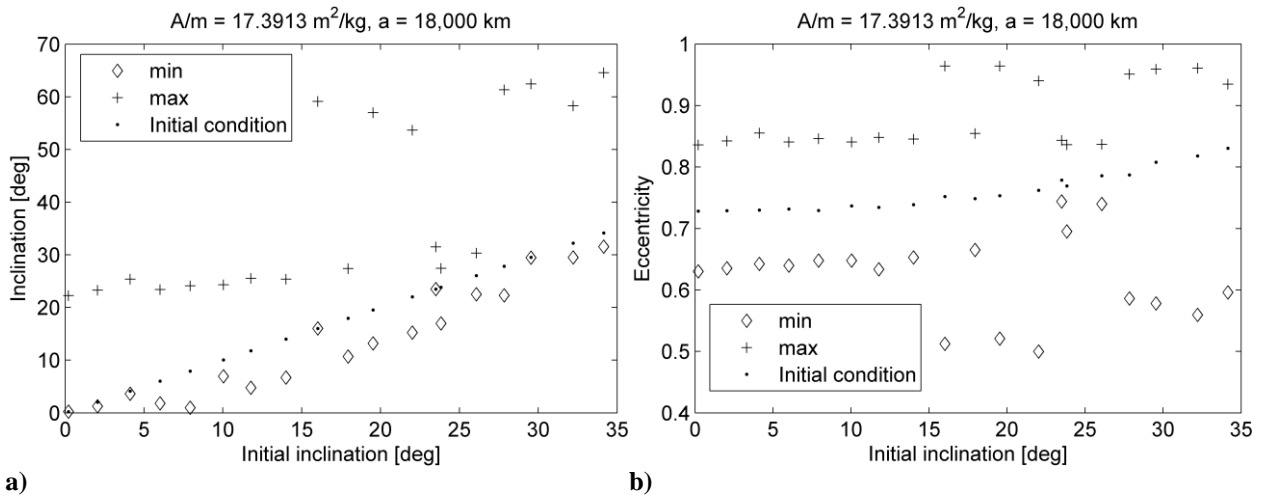
Fig. 11: Oscillation of (a) inclination and (b) eccentricity for Sun-pointing apogee orbits (Minimum: diamond; Maximum: cross). The quasi-frozen conditions (dots) are used as initial conditions for a 20 years numerical integration.

a)   b)
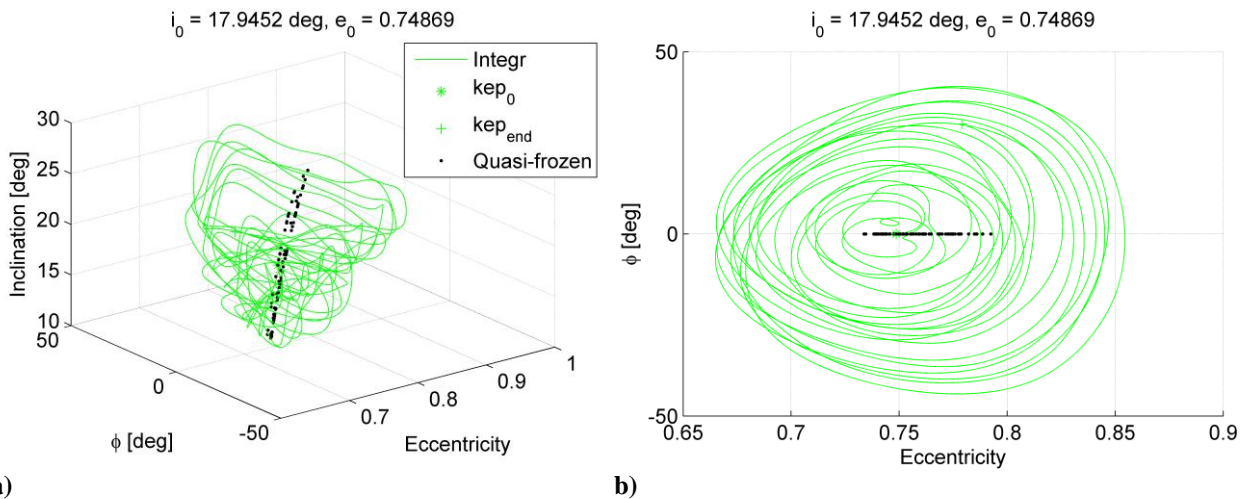
Fig. 12: Evolution of one condition of heliotropic orbit: a) 3D structure, b) planar structure.

V. HELIOTROPIC ORBITS FOR EARTH OBSERVATION

The quasi-frozen heliotropic orbits identified in Section IV give better coverage during daylight hours since at the apogee, which is always oriented in direction of the Sun, the spacecraft moves slower than at the perigee, which is always oriented away from the Sun. This effect is also strengthened by the exploitation of SRP that allows an increase in the eccentricity of the Sun-pointing apogee orbit with respect to a J_2 only orbit [17]. These findings could form the basis for a swarm of small spacecraft (i.e., CubeSats) for Earth observation or telecommunications with enhanced coverage on the day-side of the Earth. It has been demonstrated in fact that elliptical rings of spacecraft form wave-like patterns which circulate around the elliptical ring, with peaks in density at the apogee [24]. Moreover, different spacecraft can be placed into orbit with different inclinations to cover an extended range of latitudes on the Earth's surface. Such families of orbits are here designed considering a spacecraft with an area-to-mass of 10 m²/kg (i.e., a 30 kg mass spacecraft would require 9-meters-radius circular reflecting surface), reflectivity coefficient of 1.8 and orbiting at a semi-major axis of 12,000 km. This choice of parameters ensures, from Fig. 3, that the heliotropic equilibrium will be at $e < e_{crit}$. The numerical search in Eq. (7) provides the initial conditions for heliotropic elliptical and inclined orbits represented with the green dots in Fig. 13.
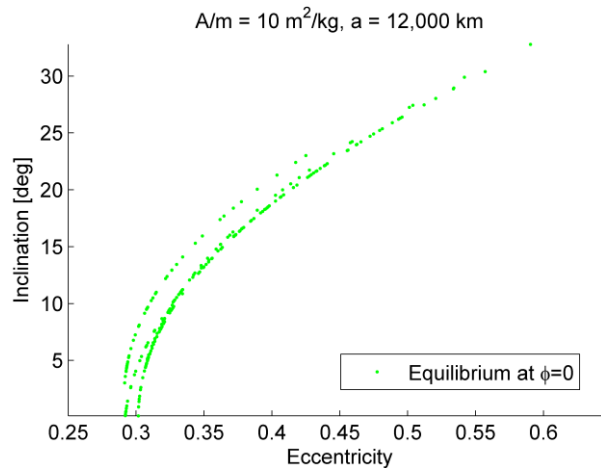
Fig. 13: Quasi-frozen orbits at non-zero inclination under SRP and J_2 for A/m = 10 m²/kg and a = 12,000 km: sun-pointing apogee orbits (green).

For this set of initial conditions the long term integration over a period of 20 years shows small oscillations in the eccentricity, solar radiation-perigee angle ϕ and inclination around the initial quasi-frozen value. This is clearly visible in Fig. 14 which represents the result of the numerical evolution (green lines) of some initial conditions chosen at different inclinations among the quasi-frozen conditions (black dots). The maximum and minimum of the oscillation around the initial value of eccentricity and inclination are reported in Fig. 15.

a)   b)
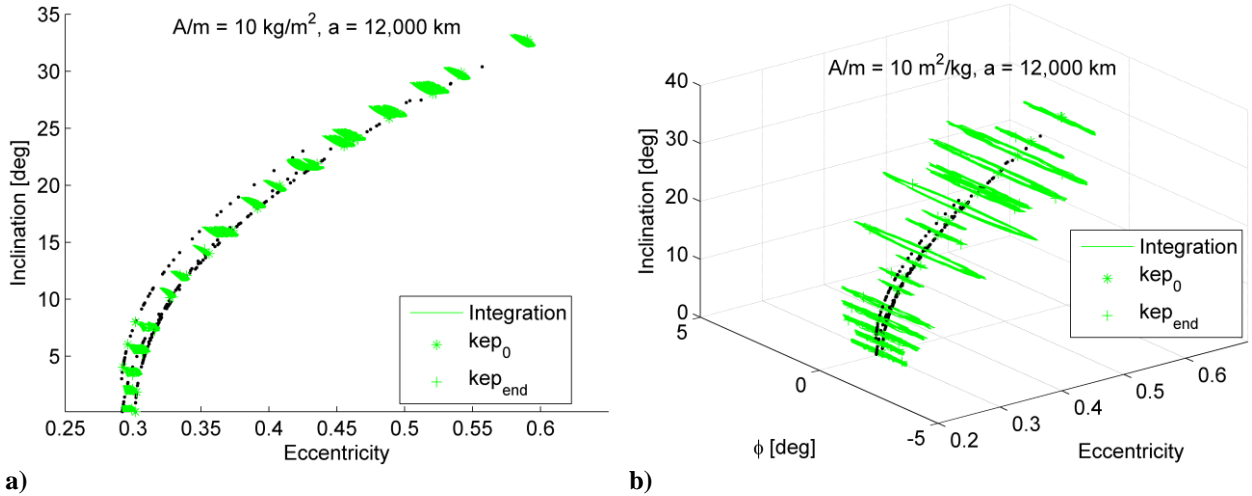
Fig. 14: **Long term evolution of quasi-frozen orbits at non-zero inclination under SRP and J_2 for A/m = 10 m^2/kg and a = 12,000 km: sun-pointing apogee orbits (green). a) Eccentricity-inclination and b) eccentricity-ϕ-inclination.**

a)   b)
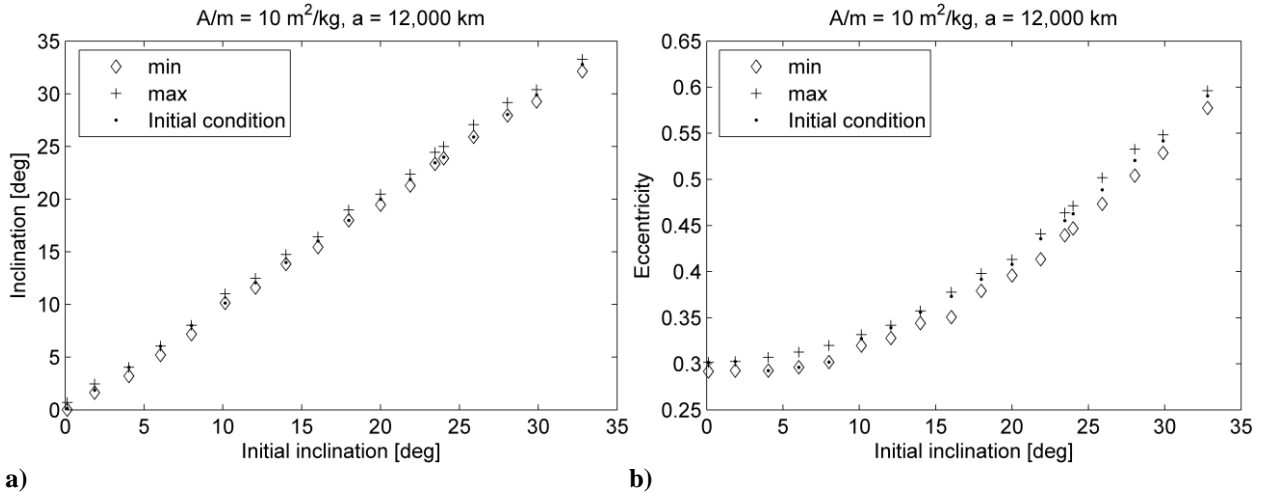
Fig. 15: **Oscillation of a) inclination and b) eccentricity for Sun-pointing apogee orbits (Minimum: diamond; Maximum: cross). The quasi-frozen conditions (dots) are used as initial conditions for a 20 years numerical integration.**

The choice of the initial orbit inclination over the equator directly determines the maximum and minimum declination that the spacecraft reaches over the equator as shown in Fig. 16. We are interested in the position of the orbit apogee with respect to the equator, where the spacecraft will spend a major fraction of its orbit (this fraction being determined by the orbit eccentricity). Therefore, the right ascension and declination of the osculating apogee point are computed, as defined in Fig. 17.
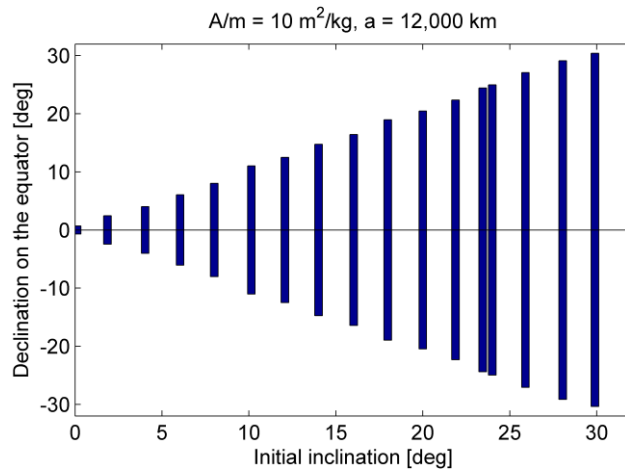
Fig. 16: Maximum and minimum declination of the osculating apogee over the equator.
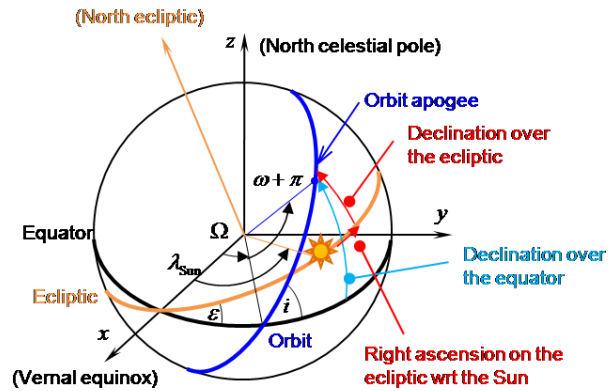
Fig. 17: 3D orbit geometry, right ascension and declination.

In the following, two examples heliotropic orbits are analysed, respectively at low and medium inclination. These orbit designs allow covering respectively a low or medium latitude band on the Earth.

V.I. Low-latitude band

A low-latitude band heliotropic orbit is chosen with initial conditions: $i_0 = 6.04\,\mathrm{deg}$ and $e_0 = 0.29$. This orbit evolves with small oscillations of the inclination around the initial condition (see Fig. 18). The planar structure is clearly visible in the eccentricity-ϕ phase space reported in Fig. 19.
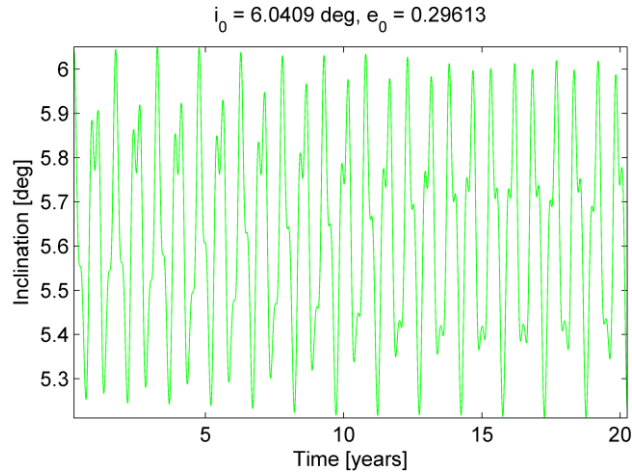
Fig. 18: Long-term evolution of the inclination for low-inclination heliotropic orbit.
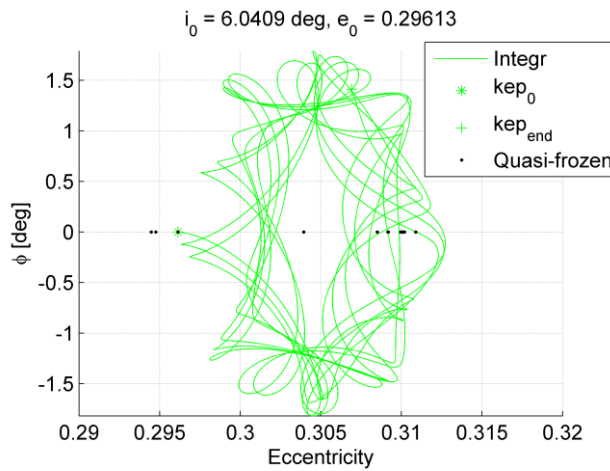
Fig. 19: Eccentricity-ϕ phase space for low-inclination heliotropic orbit.

The evolution of the heliotropic orbit over a period of 1 year is represented in Fig. 20a-c in a reference system whose *x-y* plane is on the Earth equator, with its x-axis pointing in the direction of the Sun radiation throughout the year (sun in −*x* direction at infinity). As can be seen the apogee is always directed along the Sun-direction and the orbit describes a torus around the Earth. As expected, the spacecraft on this orbit covers an equatorial band on the Earth surface. This is visible in Fig. 20d which represents the groundtrack of the osculating apogee on the Earth surface over a period of 20 years. Note that, in this figure, the map of the Earth has been under-imposed with the only purpose of indicating the latitude band covered by the apogee sub-point and the Earth rotation beneath is not yet considered at this stage of the orbit design. Future work will deal with the orbit period selection for repeated groundtrack. The choice of this initial inclination would allow for example the monitoring of the latitude range of the Amazon and other tropical rainforests in visible light.
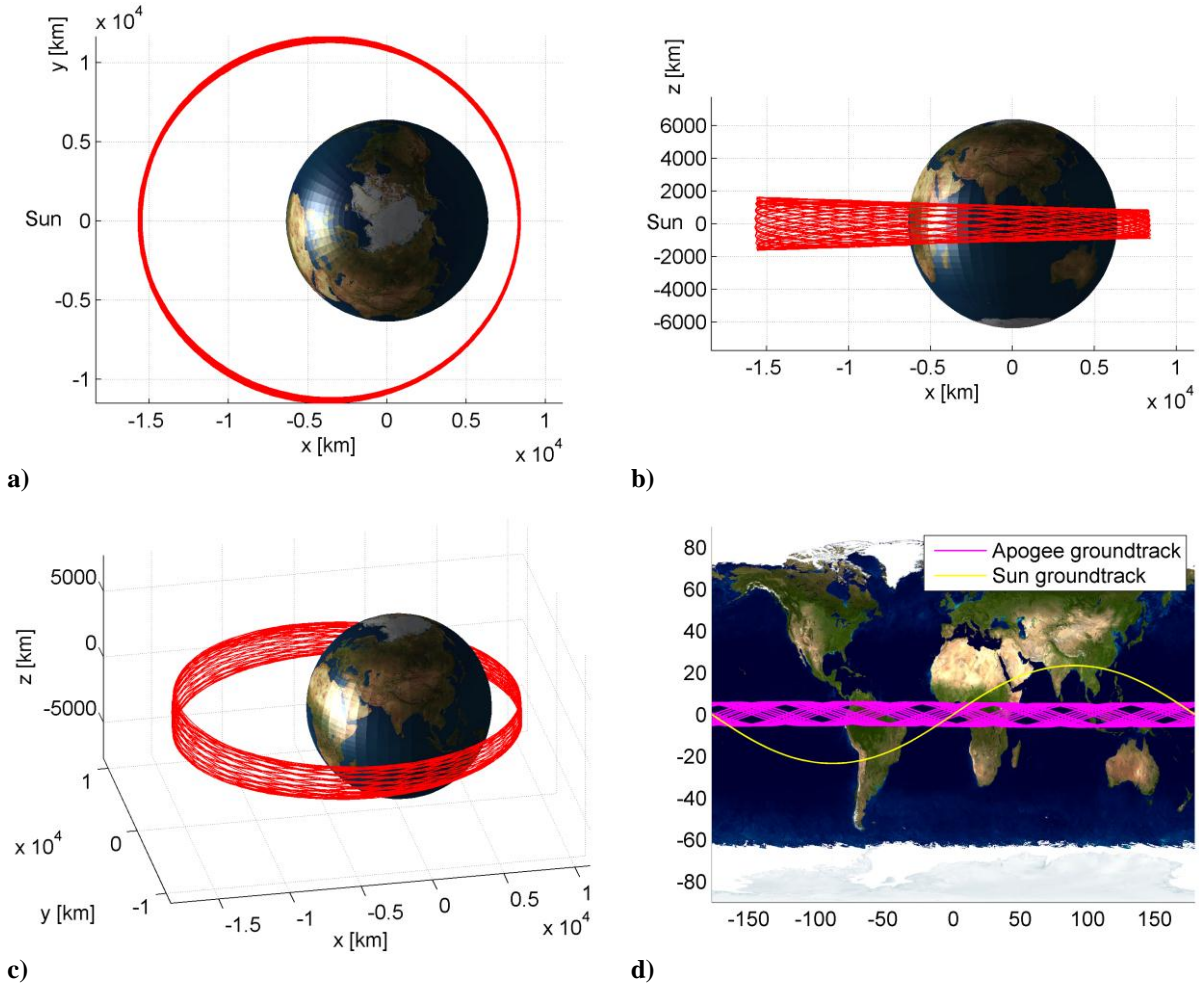
Fig. 20: Orbit evolution in an Earth-centred system with the negative *x*-axis pointing in direction of the Sun and groundtrack of the osculating orbit apogee for low-inclination heliotropic orbit.

Finally, Fig. 21 represents the declination of the osculating apogee point with respect to the ecliptic and the right ascension measured on the ecliptic with respect to the Sun. The apogee point oscillates above or below the Sun approximately within the range $\left[-\varepsilon-i_0, \varepsilon+i_0\right]$ depending on the seasons (see Fig. 21a). Remarkably, the apogee point is always Sun-facing as shown in Fig. 21b. As a consequence, the spacecraft will be covering the dayside of the Earth when transiting through the apocentre.

a)   b)
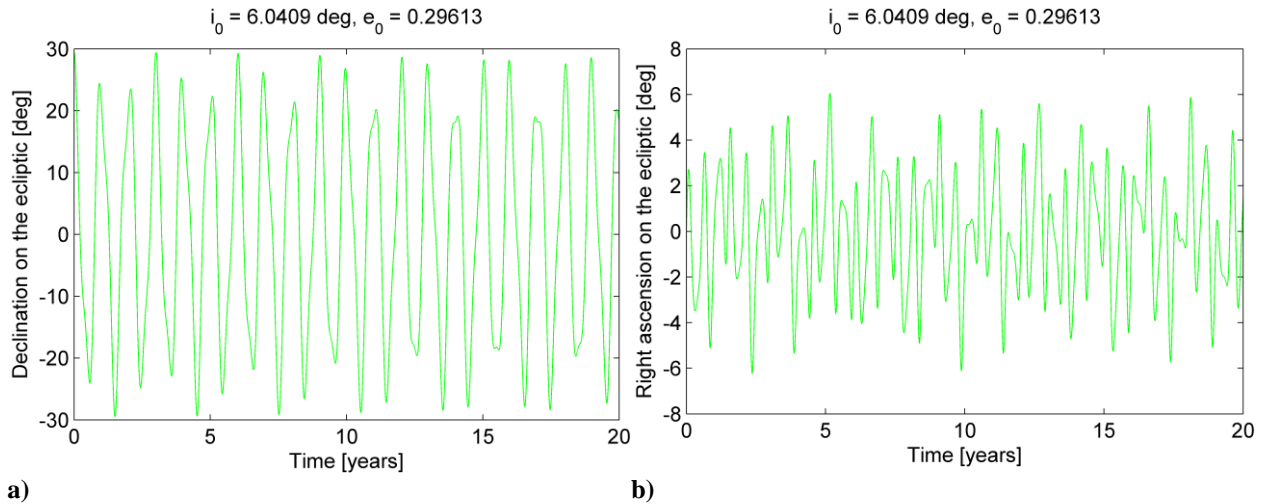
Fig. 21: Osculating apogee-Sun angles for low-inclination heliotropic orbit. a) Declination with respect to the Sun and b) right ascension on the ecliptic measured from the Sun.

V.II. Medium-latitude band

The second orbit presented is a heliotropic orbit with initial conditions $i_0 = 21.8\,\text{deg}$ and $e_0 = 0.44$. Also in this case the inclination with respect to the equatorial system is limited to ± 0.5 degrees from the initial inclination (see Fig. 22) and the planar structure in the eccentricity-ϕ phase is still recognisable even if the initial inclination is quite high (see Fig. 23).
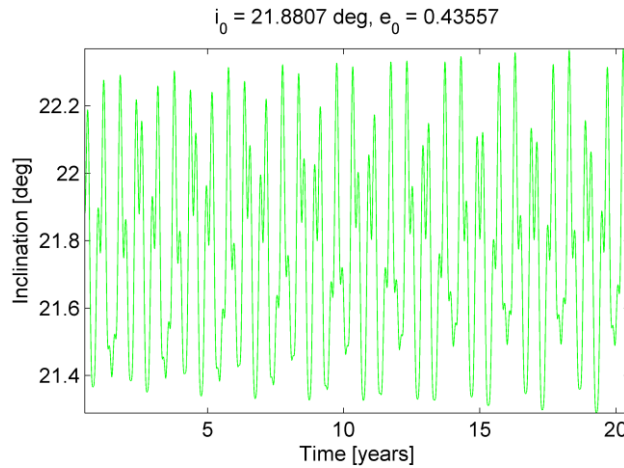
Fig. 22: Long-term evolution of the inclination for medium-inclination heliotropic orbit.
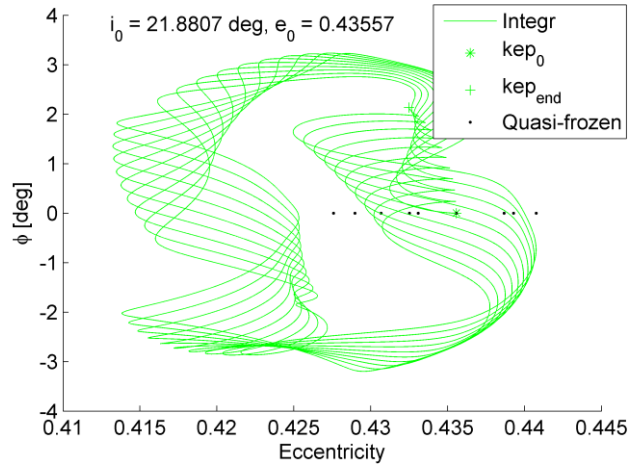
Fig. 23: Eccentricity-ϕ phase space for medium-inclination heliotropic orbit.

The latitude band covered in this case includes low and medium latitudes throughout the year (see Fig. 24d). The apogee point in fact will rotate in the orbit plane which maintains a quasi-constant inclination with respect to the equatorial plane (the argument of the ascending node is changing, but also the argument of perigee such that the true longitude of the apogee point is following the Sun's apparent rotation). Fig. 25 represents the declination of the osculating apogee point with respect to the ecliptic and the right ascension measured on the ecliptic with respect to the Sun.

a)

b)

c)   d)
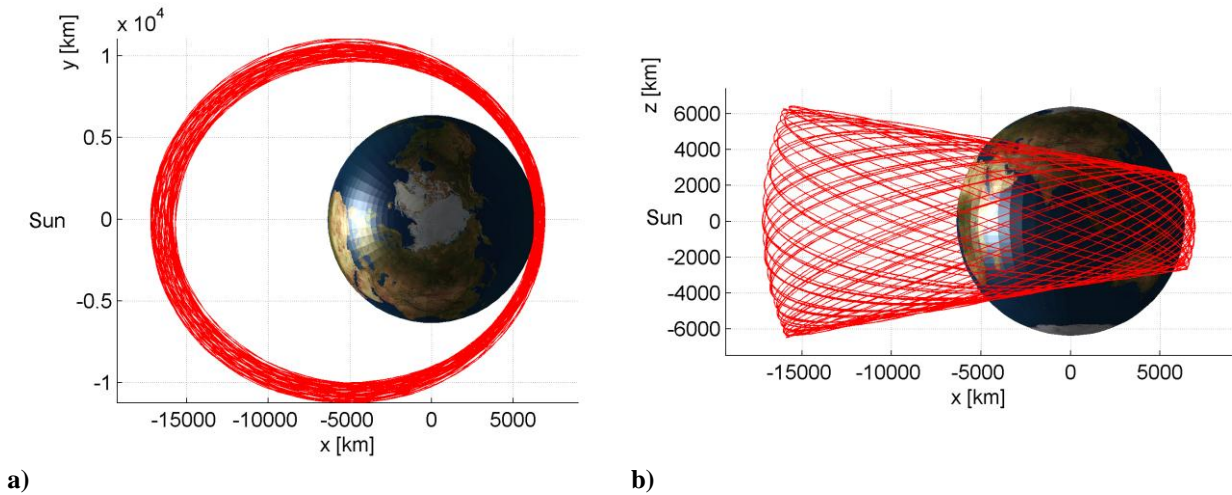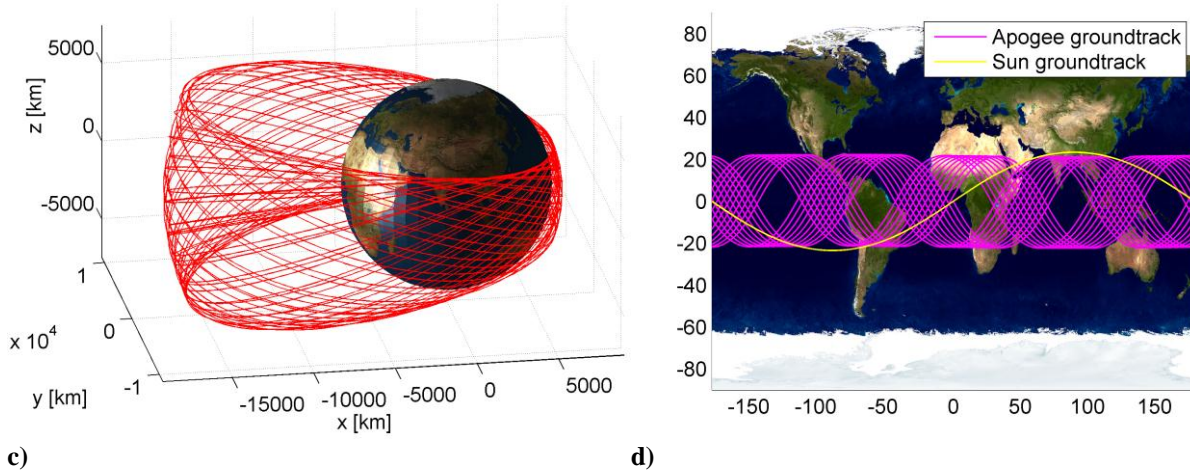
Fig. 24: Orbit evolution in an Earth-centred system with the negative *x*-axis pointing in direction of the Sun and groundtrack of the osculating orbit apogee for medium-inclination heliotropic orbit.

a)   b)
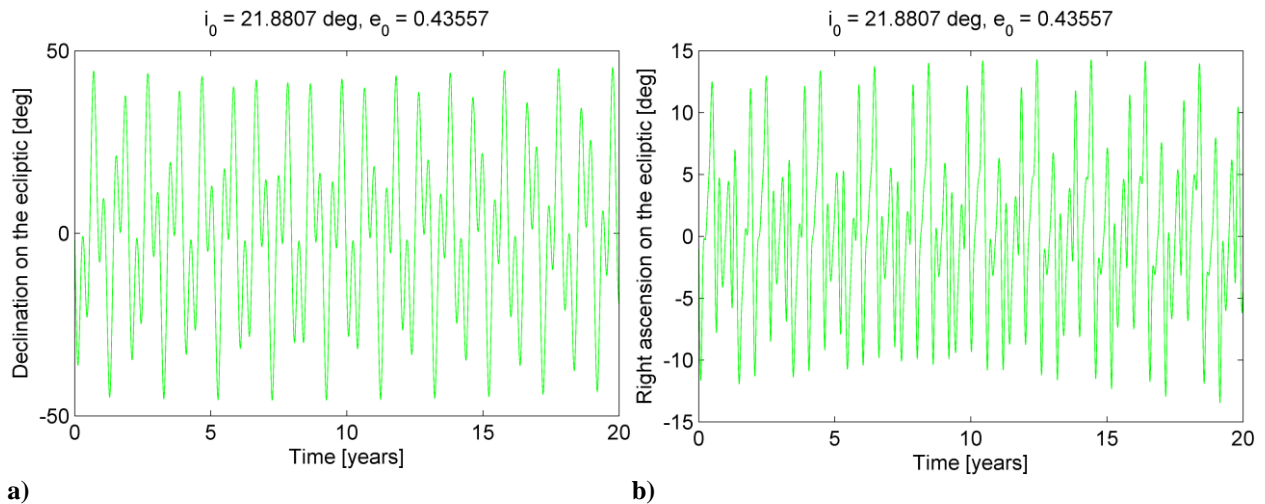
Fig. 25: Osculating apogee-Sun angles for medium-inclination heliotropic orbit. a) Declination with respect to the Sun and b) right ascension on the ecliptic measured from the Sun.

VI. CONCLUSIONS

This paper extends the analysis of the effect of solar radiation pressure and planetary oblateness to inclined orbits of high area-to-mass spacecraft. By employing a full three-dimensional model of the dynamics, initial conditions for quasi-frozen orbits are found. In the case of J_2 only an analytical solution for a Sun-following orbit is found where the line of apsides maintains a constant right ascension with respect to the Sun. If the apogee is chosen in the Sun-pointing direction, this allows enhanced dayside coverage of the Earth. The effect of SRP on high area-to-mass spacecraft can be used to increase the eccentricity of these orbits. In this case a set of heliotropic and antiheliotropic orbit are found, where the osculating apogee points respectively towards or away from the Sun. Such families of orbits can be used for a wide range of applications geomagnetic tail studies (antiheliotropic) or geoengineering [8], telecoms, daylight observation and space solar power (heliotropic). Finally, a set of heliotropic inclined orbits are developed for the observation and telecoms of a low and medium latitude bands on the Earth. A network of small spacecraft can be placed on different

orbit inclinations to increase day-side coverage. Moreover, additional constraints can be imposed on the semi-major axis to time the spacecraft passage through the apogee with the Earth's rotation. In this way the spacecraft swarm will passively cluster near apogee to provide a higher density of observations of the dayside of the Earth for visible light imaging or the provision of telecommunications services during daylight hours when bandwidth demand is greatest. Future work will investigate the stability of these orbits and derive a semi-analytical model for the amplitude and the period of the oscillations of inclination.

ACKNOWLEDGMENTS

VII. REFERENCES

[1] Graziano, M., Cadenas, R., Medina, A., Puiatti, A., Mura, M., Puccinelli, D., Barrientos, A., Rossi, C., Sanz, D. and Dufour, J.-F., "Distributed Instruments in Preparation to Manned Missions to Mars and Moon," *61st International Astronautical Congress*, Prague, 2010, IAC-10-D3.2.9.

[2] Vladimirova, T., Xiaofeng, W. and Bridges, C. P., "Development of a Satellite Sensor Network for Future Space Missions," *Proceedings of the Aerospace Conference, 2008 IEEE*, 2008, pp. 1-10.

[3] Warneke, B. A. and Pister, K. S. J., "Mems for Distributed Wireless Sensor Networks," *Proceedings of the 9th International Conference on Electronics, Circuits and Systems*, Vol. 1, 2002, pp. 291-294.

[4] Atchison, J. A. and Peck, M. A., "A Passive, Sun-Pointing, Millimeter-Scale Solar Sail," *Acta Astronautica*, Vol. 67, No. 1-2, 2010, pp. 108-121. doi: 10.1016/j.actaastro.2009.12.008

[5] Barnhart, D. J., Vladimirova, T. and Sweeting, M. N., "Very-Small-Satellite Design for Distributed Space Missions," *Journal of Spacecraft and Rockets*, Vol. 44, No. 6, 2007, pp. 1294-1306. doi: 10.2514/1.28678

[6] Shapiro, I. I., Jones, H. M. and Perkins, C. W., "Orbital Properties of the West Ford Dipole Belt," *Proceedings of the IEEE*, Vol. 52, No. 5, 1964, pp. 469-518.

[7] Colombo, C. and McInnes, C., "Orbit Design for Future Spacechip Swarm Missions in a Planetary Atmosphere," *Acta Astronautica*, Vol. 75, No. 0, 2012, pp. 25-41. doi: 10.1016/j.actaastro.2012.01.004

[8] Bewick, R., Lücking, C., Colombo, C., Sanchez, J. P. and McInnes, C. R., "Geo-Engineering Using Dust Grains in Heliotropic Elliptical Orbits," *62nd International Astronautical Congress*, Cape Town, 2011, IAC-11-D1.1.9.

[9] Atchison, J. A. and Peck, M. A., "Length Scaling in Spacecraft Dynamics," *Journal of Guidance, Control, and Dynamics*, Vol. 34, No. 1, 2011, pp. 231-246. doi: doi: 10.2514/1.49383

[10] Colombo, C. and McInnes, C., "Orbital Dynamics of 'Smart Dust' Devices with Solar Radiation Pressure and Drag," *Journal of Guidance, Control, and Dynamics*, Vol. 34, No. 6, 2011, pp. 1613-1631. doi: 10.2514/1.52140

[11] Hamilton, D. P. and Krivov, A. V., "Circumplanetary Dust Dynamics: Effects of Solar Gravity, Radiation Pressure, Planetary Oblateness, and Electromagnetism," *Icarus*, Vol. 123, No. 2, 1996, pp. 503-523. doi: 10.1006/icar.1996.0175

[12] Horányi, M. and Burns, J. A., "Charged Dust Dynamics: Orbital Resonance Due to Planetary Shadows," *J. Geophys. Res.*, Vol. 96, No. A11, 1991, pp. 19283-19289. doi: 10.1029/91ja01982

[13] Krivov, A. V., Sokolov, L. L. and Dikarev, V. V., "Dynamics of Mars-Orbiting Dust: Effects of Light Pressure and Planetary Oblateness," *Celestial Mechanics and Dynamical Astronomy*, Vol. 63, No. 3, 1995, pp. 313-339. doi: 10.1007/bf00692293

[14] Hedman, M. M., Burt, J. A., Burns, J. A. and Tiscareno, M. S., "The Shape and Dynamics of a Heliotropic Dusty Ringlet in the Cassini Division," *Icarus*, Vol. 210, No. 1, 2010, pp. 284-297.

[15] Burt, J., Hedman, M. M., Burns, J. A. and Tiscareno, M. S., "Dynamical Analysis of the Heliotropic "Charming" Ringlet in Saturn's Cassini Division," *American Astronomical Society, DDA meeting #41, #11.08; Bulletin of the American Astronomical Society*, Vol. 41, 2010, p. 940.

[16] Krivov, A. V. and Getino, J., "Orbital Evolution of High-Altitude Balloon Satellites," *Astron. Astrophys.*, No. 318, 1997, p. 7.

[17] Draim, J. E., Cefola, P. and Castrel, D., "Elliptical Orbit Constellations-a New Paradigm for Higher Efficiency in Space Systems?," *Proceedings of the Aerospace Conference Proceedings, 2000 IEEE*, Vol. 7, 2000, pp. 27-35.

[18] Hamilton, D. P., "The Asymmetric Time-Variable Rings of Mars," *Icarus*, Vol. 119, No. 1, 1996, pp. 153-172. doi: 10.1006/icar.1996.0008

[19] Coleman, T. F. and Li, Y., "On the Convergence of Interior-Reflective Newton Methods for Nonlinear Minimization Subject to Bounds," *Mathematical Programming*, Vol. 67, No. 1, 1994, pp. 189-224.

[20] Coleman, T. F. and Li, Y., "An Interior Trust Region Approach for Nonlinear Minimization Subject to Bounds," *SIAM Journal on Optimization*, Vol. 6, No. 2, 1996, pp. 418-445.

[21] Vallado, D. A., *Fundamentals of Astrodynamics and Applications*, Third Edition, Space Technology Library, New York, 2007.

[22] Dormand, J. R. and Prince, P. J., "A Family of Embedded Runge-Kutta Formulae," *Journal of computational and applied mathematics*, Vol. 6, No. 1, 1980, pp. 19-26.

[23] Colombo, C. and McInnes, C. R., "Evolution of Swarms of 'Smart Dust' Spacecraft," *Proceedings of the New Trends in Astrodynamics and Applications VI*, Courant Institute of Mathematical Sciences, New York University, 2011.

[24] McInnes, C. R. and Colombo, C., "Wave-Like Patterns in an Elliptical Satellite Ring," *in press Journal of Guidance, Control, and Dynamics*, 2012.

VIII. VITAE

Camilla Colombo is Lecturer in Spacecraft Engineering at the University of Southampton. Previously she was Research Fellow at the Advanced Space Concepts Laboratory at the University of Strathclyde. Her research focuses on the orbital dynamics of high area-to-mass spacecraft, space trajectory design and optimisation, and asteroid deflection. Previously, she was appointed as research associate at the Department of Aerospace Engineering of the University of Glasgow, where she completed her Ph.D. on Optimal Trajectory Design for Interception and Deflection of Near Earth Objects and was awarded the William Wilson Scott Award Scholarship (2009). She received her MSc in Aerospace Engineering at Politecnico di Milano with a thesis on optimisation method for low-thrust trajectories.

Charlotte Lücking is a final year Ph.D. student at the Advanced Space Concepts Laboratory at Strathclyde University. Her work focuses on space mission applications of high area-to-mass ratio orbital dynamics. In the past she has investigated the orbital dynamics and control of smart dust devices, the passive stability of dust in Earth-orbiting heliotropic orbits and solar radiation pressure-augmented deorbiting. For her work she has won several awards including the EADS Astrium Prize in Space Systems Engineering (2008/09), an IET Ambition Award (2011) and the Frank J. Redd Student Scholarship (2011).

Colin McInnes is Director of the Advanced Space Concepts Laboratory at the University of Strathclyde. His work spans highly non-Keplerian orbits, orbital dynamics and mission applications for solar sails, spacecraft control using artificial potential field methods and is reported in over 100 journal papers. Recent work is exploring new approaches to spacecraft orbital dynamics at extremes of spacecraft length-scale to underpin future space-derived products and services. McInnes has been the recipient of awards including the Royal Aeronautical Society Pardoe Space Award (2000), the Ackroyd Stuart Propulsion Prize (2003) and a Leonov medal by the International Association of Space Explorers (2007).